An electron spin resonance study of vanadium-doped alpha -TeO_2 single crystals

1995 J. Phys.: Condens. Matter 7 3013

(http://iopscience.iop.org/0953-8984/7/15/008)

J. Phys.: Condens. Matter 7 (1995) 3013–3022. Printed in the UK

An electron spin resonance study of vanadium-doped α-TeO_2 single crystals

G J Edwards†, O R Gilliam†, R H Bartram†, A Watterich‡, R Voszka‡, J R Niklas§, S Greulich-Weber§ and J-M Spaeth§

† Department of Physics and Institute of Materials Science, University of Connecticut, Storrs, CT 06269-3136, USA

‡ Research Laboratory for Crystal Physics, Hungarian Academy of Sciences, Budaörsi út 45, H-1112 Budapest, Hungary

§ University of Paderborn, Fachbereich 6, Warburger Strasse 100A, 33098 Paderborn, Germany

Received 29 December 1994

Abstract. An ESR study of vanadium-doped paratellurite indicates that vanadium enters the lattice as V^{4+}, equally populating the four inequivalent cation sites. The $3d^1$ electron exhibits hyperfine interaction with the $I = \frac{7}{2}$ ^{51}V nucleus and superhyperfine interaction with two neighbouring $I = \frac{1}{2}$ nuclei identified as protons by ENDOR experiments. Spin Hamiltonian parameters computed from ESR measurements show that each V^{4+} ion has a single C_2 symmetry axis along one of the ⟨110⟩ directions. The neighbouring hydrogens appear to enhance the symmetry and stability of the defect structure. Group theoretical arguments show that there are two possible linear combinations of d wavefunctions that could represent the ground state of V^{4+} in α-TeO_2. However, a determination of the lower-lying state was not feasible using only the ESR data.

1. Introduction

Paratellurite (α-TeO_2) is a transparent acousto-optic and piezoelectric material whose enhanced piezo-optic constant has led to practical applications in deflectors, modulators and tunable optical filters. To characterize this material, we initiated electron spin resonance (ESR), electron nuclear double resonance (ENDOR) and optical absorption studies on point defects, which consisted of impurity or dopant ions, as well as intrinsic defects generated by bombardment with fast electrons. With regard to dopant ions, paratellurite does not easily permit their inclusion into the lattice. To avoid precipitation or aggregation of foreign ions during crystal growth only a small amount of dopant material can be added to the melt. Consequently, the low dopant concentration in the crystal limits the intensities of ESR signals and often precludes optical absorption measurements. These conditions prevailed for the current study of vanadium-doped α-TeO_2 and optical absorption measurements were not feasible. Interpretation of the ESR observations shows that vanadium is present as V^{4+} substitutional for Te^{4+}; thus no charge compensation is required. However, there is evidence by ESR and ENDOR of a pair of impurity protons in the vicinity of each vanadium ion, as will be discussed. In addition, a theoretical method designed to determine the energy level scheme for V^{4+} in α-TeO_2 will be described.

0953-8984/95/153013+10$19.50

2. Background

2.1. Intrinsic defects

In earlier work the undoped paratellurite crystals gave no ESR signals before irradiation for observations at 92 K, but a 1 MeV electron irradiation at room temperature generated an intrinsic spin-$\frac{1}{2}$ defect, which was attributed to an electron trapped at an oxygen vacancy [1]. The defect was designated as a $V_0^{\cdot}$ centre (in Kröger–Vink notation [2]) with properties intermediate between those of the E_1' centre in SiO_2 [3,4] and the F^+ centre in alkaline earth oxides [5]. After prolonged electron irradiation at 1.65 MeV, two additional intrinsic defects were prominent in the ESR runs. One was identified as an oxygen divacancy with a net positive charge relative to the lattice and designated as a $(V_0)_2^{\cdot}$ centre, and the second identified as a peroxy radical, i.e., an O_2^- ion [6]. ENDOR was also used in the identification of these two defects.

2.2. Impurity ions

Electron-irradiated Al-doped paratellurite crystals indicated a family of four defects attributed to Al^{3+}-perturbed $V_0^{\cdot}$ centres [7]. Platinum was an impurity in undoped crystals, and both Pt-perturbed $V_0^{\cdot}$ centres [8,9] and Pt^{3+} substitutional cations [9] were investigated. In Cr-doped crystals, Cr^{3+} was found by ESR to occupy normal as well as perturbed cation sites [10], and electron irradiation was observed to change the Cr^{3+} ions to Cr^{5+} [11]. Optical absorption studies were made earlier on Cr-doped [12] and Fe-doped [13] paratellurite crystals.

3. The crystal structure of paratellurite

The paratellurite phase of TeO_2 has the tetragonal space group of D_4^4 ($P4_12_12$). The tetragonal crystal structure may be regarded as a distorted rutile structure with a doubling of the unit cell along the [001] direction or c axis [14] as shown in figure 1. The tellurium ion is fourfold coordinated by oxygens with two different pairs of oxygens having Te–O bond lengths 0.188 and 0.212 nm, resulting in an asymmetric trigonal bipyramid with the tellurium at its apex [15]. Two additional oxygens, which have 0.286 nm Te–O bond lengths and which are ionically bonded to the tellurium, complete an overall distorted octahedron structure. The tellurium site in the crystal is of C_2 symmetry with a diad axis along the direction bisecting the two short bonds and perpendicular to the two long bonds of the $Te–(O)_4$ base unit of the crystal. The diad axes are parallel to the $\langle 110 \rangle$ direction. Eight inequivalent oxygen sites and four inequivalent tellurium sites can be distinguished in the crystal.

4. Experimental details

High-quality paratellurite crystals were grown in Budapest by a balance-controlled Czochralski technique using a platinum crucible and resistance heating [16]. A pulling rate of 1.2 mm h^{-1} along the [110] direction and a seed rotation of 30 rpm were used. The crystals were oriented by x-ray diffraction and cut to a typical sample size of $10 \times 3.5 \times 3$ mm^3 with a diamond saw. All ESR observations were performed at the University of Connecticut using a Varian E-3 X-band spectrometer. Measurements were made at about 92 K with

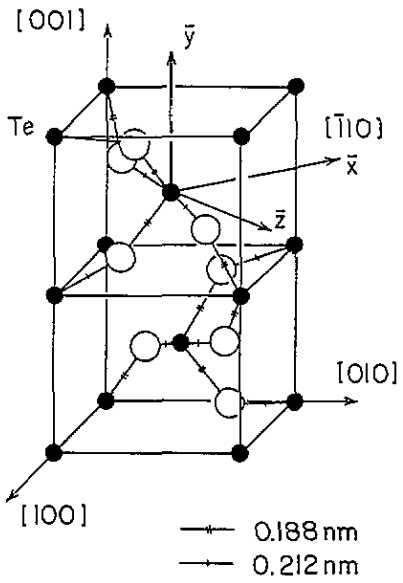

Figure 1. The crystal structure of paratellurite (α-TeO_2). The tetragonal structure may be regarded as a distorted rutile structure with a doubling of the unit cell along the [001] direction. The short and the long bonds are distinguished. The chosen axes x, y and z are consistent with typical principal axes of paramagnetic cations in regular (undistorted) rutile crystal structures.

microwave powers up to 25 mW and at a frequency of about 9.1 GHz. The ENDOR experiments were conducted at the University of Paderborn with a custom-built computer-controlled X-band spectrometer. The sample temperature could be varied between 4 and 300 K; the ENDOR frequency could be varied in the range between 0.5 and 160 MHz.

5. Experimental results

Paratellurite doped with vanadium has exhibited a spin-$\frac{1}{2}$ ESR spectrum with an eight-line hyperfine (HF) splitting, which is characteristic of interactions with ^{51}V ($I = \frac{7}{2}$, 99.8% natural abundance). In arbitrary directions, four sets of HF lines are observed, which indicates that there are four inequivalent sites for the vanadium ion. The spectra for the four sites collapse for $\boldsymbol{B}$ along the [001] and [100] directions into one set of eight HF lines; the spectrum for the former orientation is shown in figure 2(a). If $\boldsymbol{B}$ is parallel to the [110] direction, two sets of eight HF lines are obtained (not shown). For most orientations each HF line is split into four lines of equal intensity due to superhyperfine (SHF) interaction. Figure 2(b) depicts this SHF splitting for one of the HF lines, where $\boldsymbol{B}$ is slightly but increasingly misaligned from the [100] direction as one goes from the upper to the lower ESR trace. For $\boldsymbol{B} \parallel [001]$, instead of four separate lines, the SHF structure appears as three lines with the intensity ratios 1:2:1, as shown for a single HF line in figure 2(c). This suggests that the SHF splitting results from interactions with two spin-$\frac{1}{2}$ nuclei that are equivalent for this orientation.

The spin Hamiltonian for this system can be expressed as

$$\mathcal{H}_s = \mathcal{H}_0 + \mathcal{H}_1 \tag{1}$$

where $\mathcal{H}_0$ for $S = \frac{1}{2}$ and $I = \frac{7}{2}$ is given by the spin Hamiltonian

$$\mathcal{S}_0 = \mu_B \boldsymbol{B} \cdot \mathbf{g} \cdot \boldsymbol{S} + \boldsymbol{S} \cdot \mathbf{A} \cdot \boldsymbol{I} + \boldsymbol{I} \cdot \mathbf{P} \cdot \boldsymbol{I} - g_N \mu_N \boldsymbol{B} \cdot \boldsymbol{I} \tag{2}$$

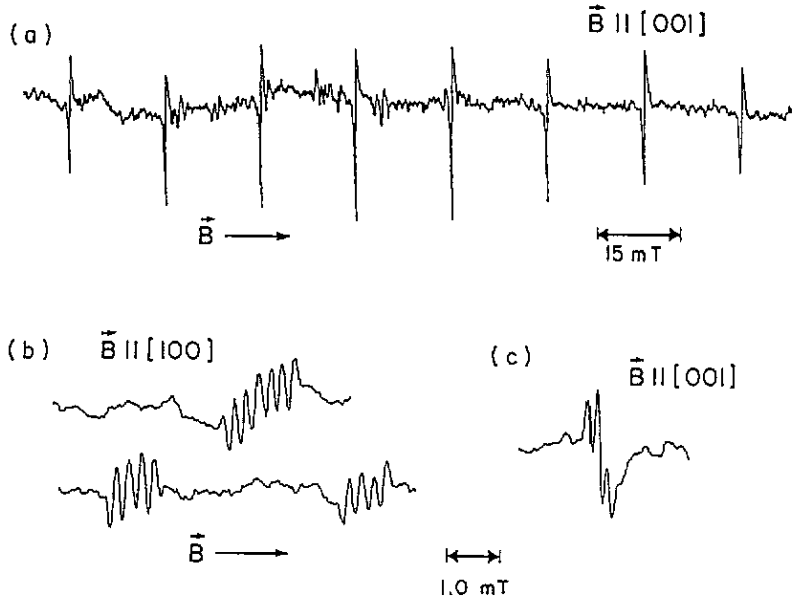

Figure 2. ESR spectra of α-TeO_2:V^{4+} along specific axes. (a) An eight-line HF structure is shown for $B \parallel [001]$. (b) SHF interactions split each HF line into four lines of equal intensity. For the upper ESR trace the magnetic field B is only slightly shifted from the [100] direction. For the lower trace the shift of B from [100] is greater. (c) A single HF line where the SHF interactions cause a three-line pattern with 1:2:1 intensity ratios for $B \parallel [001]$.

and the SHF interactions are given by

$$\mathcal{H}_1 = \boldsymbol{S} \cdot \mathbf{A}' \cdot \boldsymbol{I}' - g'_N \mu_N \boldsymbol{B} \cdot \boldsymbol{I}' + \boldsymbol{S} \cdot \mathbf{A}'' \cdot \boldsymbol{I}'' - g''_N \mu_N \boldsymbol{B} \cdot \boldsymbol{I}'' \tag{3}$$

where $\mathbf{A}'$ and $\mathbf{A}''$ are tensors describing the SHF interactions with nuclear spins $\boldsymbol{I}'$ and $\boldsymbol{I}''$, respectively, and g'_N and g''_N are the respective nuclear g values.

Angular variation measurements were made in both the (010) and $(\bar{1}10)$ planes to determine the best-fit spin Hamiltonian parameters $\mathbf{g}$, $\mathbf{A}$ and $\mathbf{P}$ neglecting SHF splittings. These measurements are shown as data points in figure 3(a) and (b), respectively. The solid lines are computer-simulated angular variations using the optimized parameters. The angular variation for rotation in the (010) plane (figure 3(a)) shows a splitting into *two* eight-line HF patterns of equal intensity since the four inequivalent Te sites become pairwise equivalent in this plane. In the $(\bar{1}10)$ plane (figure 3(b)) the HF lines split into *three* eight-line patterns one of which has twice the intensity of each of the other two. The eigenvalues and eigenvectors of the computer-fitted $\mathbf{g}$, $\mathbf{A}$ and $\mathbf{P}$ tensors are given in table 1, where the direction cosines correspond to the orientations of the x, y and z principal axes relative to the crystallographic axes [100], [010] and [001], respectively. The calculated values for the magnetic field strength deviate from the measured data points by an average of 0.23 mT per point. The estimated uncertainty in g values is ± 0.0005; in A values, $\pm 0.01 \times 10^{-4}$ cm^{-1}; and in P values, $\pm 0.3 \times 10^{-4}$ cm^{-1}.

The character of the SHF splittings indicated that they resulted from weak interactions with two $I = \frac{1}{2}$ nuclei. Since the splittings were small (varying from 0.2 to 0.6 mT) and the signal to noise ratios were also small, the determinations of $\mathbf{A}'$ and $\mathbf{A}''$ showed

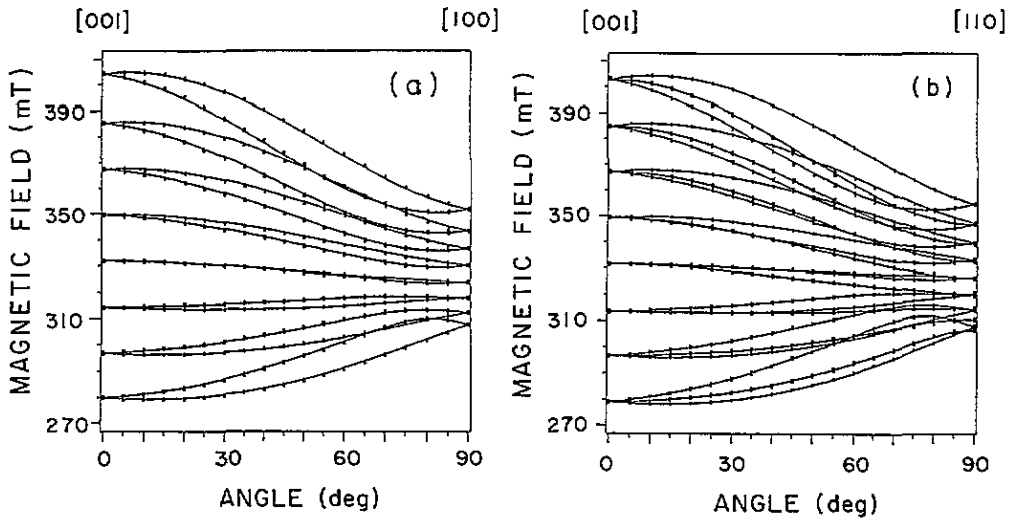

Figure 3. The angular variation of vanadium-doped paratellurite in the (a) (010) and (b) ($\bar{1}$10) planes. The points are experimental data and the solid lines are computer simulated, based on best-fit parameters of the spin Hamiltonian.

Table 1. The principal values and direction cosines of the optimized **g**, **A** and **P** tensors for vanadium-doped paratellurite, with A and P values in units of 10^{-4} cm^{-1}. The direction cosines from the top down are defined with respect to the crystallographic axes [100], [010] and [001], respectively.

g_{xx}	g_{yy}	g_{zz}	A_{xx}	A_{yy}	A_{zz}	P_{xx}	P_{yy}	P_{zz}
1.9821	1.9011	1.9491	53.03	160.13	52.07	−0.2	1.0	−0.8
0.707	−0.087	0.702	0.707	−0.142	0.693	0.71	−0.19	0.67
−0.707	−0.087	0.702	−0.707	−0.142	0.693	−0.71	−0.20	0.69
0.000	0.993	0.123	0.000	0.980	0.201	0.01	0.96	0.28

appreciable uncertainty and are not given at this time. Observations did signify, however, that the two nuclei responsible for the SHF are symmetrically positioned about the V^{4+} ion. To determine the isotope causing the SHF interactions, an ENDOR experiment was conducted. The ENDOR spectrum, shown in figure 4 for $B \parallel [001]$, exhibited two ENDOR peaks centred around a frequency of 15.53 MHz. This centre frequency is in close agreement with the proton resonance frequency of 15.564 MHz predicted for the measured magnetic field of 365.56 mT. The ENDOR measurement was performed at a temperature of 5.5 K and a microwave frequency of 9.4725 GHz. The separation of the two peaks for $B \parallel [001]$ is about 5.31 MHz and is a measure of the SHF interaction for this orientation. This interaction can be expressed as $A_{SHF} = 5.31$ MHz $= 0.205$ mT $= 1.77 \times 10^{-4}$ cm^{-1}, which confirms the less precise measurement of 0.2 mT made by ESR.

6. Discussion

6.1. Interpretation from ESR and ENDOR

It is deduced that vanadium enters the paratellurite crystal as a V^{4+} ion occupying a Te^{4+}

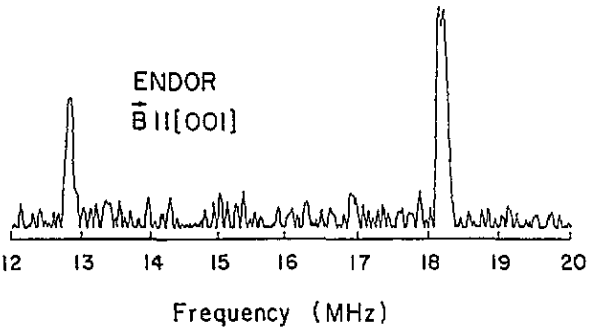

Figure 4. The ENDOR spectrum of the SHF splitting in TeO_2:V^{4+}, which is attributed to hydrogen nuclei. Measurements were made at 365.56 mT, 9.4725 GHz and 5.5 K. The peaks are centred around 15.53 MHz, compared to 15.564 MHz predicted for protons.

site. This is consistent with the experimental evidence, which signifies a spin-$\frac{1}{2}$, $I = \frac{7}{2}$ defect in four inequivalent sites. Furthermore, V^{4+} has the same charge as the tellurium cation and therefore requires no charge compensation. It is apparent that each of spin Hamiltonian tensors (**g**, **A** and **P** in table 1) has a set of direction cosines indicating a common major axis along [$\bar{1}$10], the diad axis. In table 2 we compare the spin Hamiltonian parameters for V^{4+} in paratellurite with those reported for this ion in GeO_2 [17], SnO_2 [18] and TiO_2 [19], where the principal axes for rutile-like crystals are given in brackets. The *paratellurite* V^{4+} *eigenvectors are specified relative to the crystallographic axes [100], [010]* and [001]. One notes that the direction cosines for the **g** and **A** tensors of V^{4+} in TeO_2 are shifted slightly from those reported for the rutile-like crystals; however, there is a significant change. The principal axes have been permuted in that the unique axes for **g** and **A** are different in paratellurite (where they are close to [001]) and in rutile structures (where they are along [110]). Also **g** and **A** do not have the same principal axes, which contrasts with findings in undistorted rutile structures and reflects the lowered site symmetry for V^{4+} in TeO_2. From table 3 it is seen that this change of principal axes from those of rutile is a general feature of impurity ions in paratellurite. The results indicate that the lowest-lying d wavefunction is reoriented from the xy plane in rutile to approximately the xz plane in paratellurite. This should be reflected in the ground state wave vector.

Table 2. Principal values and eigenvectors for $3d^1$ ions in rutile-type hosts. A values are in units of 10^{-4} cm^{-1}.

Host	Impurity	g_{xx} [$\bar{1}$10]	g_{yy} [001]	g_{zz} [110]	A_{xx} [$\bar{1}$10]	A_{yy} [001]	A_{zz} [110]	Reference
GeO_2	V^{4+}	1.9467	1.9211	1.9638	18.39	37.27	134.66	[17]
SnO_2	V^{4+}	*1.939*	*1.903*	*1.943*	*21.2*	*41.8*	*140.1*	*[18]*
TiO_2	V^{4+}	1.915	1.9135	1.9565	31.5	43	142	[19]
TeO_2	V^{4+}	1.9821	1.9011	1.9491	53.03	160.13	52.07	Present work
		0.707	−0.087	0.702	0.707	−0.142	0.693	
		−0.707	−0.087	0.702	−0.707	−0.142	0.693	
		0.000	0.993	0.123	0.000	0.980	0.201	

Table 3. A comparison of principal values and eigenvectors for impurity ions occupying cation sites in paratellurite. (The eigenvectors are transformed such that they correspond to the same cation site.) Only the V^{4+} ion requires no charge compensation and has two neighbouring protons. The other ions have non-local charge compensators, which do not disturb the C_2 symmetry. The V^{4+} ion with neighbouring protons has eigenvectors closest to those of the substitutional cation in rutile. A values are in units of 10^{-4} cm^{-1}.

Impurity	g_{xx}	g_{yy}	g_{zz}	A_{xx}	A_{yy}	A_{zz}	Reference
V^{4+}–2H	1.9821	1.9011	1.9491	53.03	160.13	52.07	Present work
	0.707	−0.087	0.702	0.707	−0.142	0.693	
	−0.707	−0.087	0.702	−0.707	−0.142	0.693	
	0.000	0.993	0.123	0.000	0.980	0.201	
Pt^{3+}	1.9388	2.5976	2.0996	46	191	69	[9]
	0.707	−0.215	0.673	0.707	−0.230	0.669	
	−0.707	−0.215	0.673	−0.707	−0.230	0.669	
	0.000	0.952	0.305	0.000	0.946	0.326	
Cr^{3+}	1.980	1.976	1.983				[10]
	0.707	−0.127	0.696				
	−0.707	−0.127	0.696				
	0.000	0.984	0.180				
Cr^{5+}	1.9346	1.9792	1.9725				[11]
	0.707	−0.261	0.657				
	−0.707	−0.261	0.657				
	0.000	0.930	0.369				

Even though the V^{4+} substituting for Te^{4+} requires no charge compensation, there is an SHF interaction with two $I = \frac{1}{2}$ nuclei and ENDOR measurements indicate that the nuclei are protons. The ESR measurements show that (within experimental error) the two protons give equivalent SHF interactions. Since the C_2 symmetry of the defect site is left intact, it is also apparent from the spin Hamiltonian that the protons are placed symmetrically around the diad axis. A comparison (see table 3) of the principal axes for V^{4+} in TeO_2 with the principal axes for other impurity ions in TeO_2 that do *not* show proton SHF splitting indicates that the TeO_2:V^{4+} eigenvectors are less modified from those found in the rutile structure. The protons therefore are believed to cause a more symmetric environment for impurity cations, and probably shift the oxygens surrounding the vanadium ion to more rutile-like positions. In the table only those impurity ions that exhibit C_2 symmetry are included for comparison. Other impurity cations that require local charge compensations, such as oxygen vacancies, have lower site symmetry (C_1) and are not listed. At the time of this research, no vanadium ions have been detected without a hydrogen presence; thus it can be conjectured that the higher symmetry caused by the presence of the protons may be necessary for the vanadium cation substitution to occur.

The introduction of hydrogen into the TeO_2 crystals as OH^- ions is a reasonable assumption since the crystals were grown in air; however, no infrared (IR) absorption band due to OH stretching could be found. This is interpreted by assuming the presence of very broad IR bands, broadened by hydrogen bridging. The O–O distances in TeO_2 are close to the usual O–H...O bridging distances, which range in various materials from 0.24 to

0.31 nm [20]. Thus the oxygen spacings in TeO_2 should be convenient for bridging even in the neighbourhood of the vanadium ion.

6.2. Theoretical analysis

A theoretical treatment of nd^1 ions in crystals of rutile structure has been reported by Shimizu [21, 22]. In rutile the five d orbitals transform as the following irreducible representations of D_2: A: $3z^2 - r^2$, B_1: xy, B_2: xz, B_3: yz and A: $x^2 - y^2$. Analysis of ESR and optical data established that the ground state is of A symmetry and is predominantly $x^2 - y^2$. In paratellurite the site symmetry is further reduced to C_2 with the single symmetry axis oriented along the $[\bar{1}10]$ direction (see figure 1). The orbitals then transform as the following representations of C_2: A: $3z^2 - r^2$, B: xy, A: yz, B: xz and A: $x^2 - y^2$. It is not clear *a priori* which of the two possible linear combinations of d orbitals is associated with the ground state, since the principal values of the hyperfine tensor listed in table 1 are compatible with a ground state wavefunction predominantly either xz (B symmetry), or $x^2 - y^2$ or $3y^2 - r^2$, both of which can be expressed as linear combinations of $x^2 - y^2$ and $3z^2 - r^2$ (A symmetry). If one adopts the conventional assumption that the spin–orbit interaction and the low-symmetry components of the crystal field can be treated as perturbations on the octahedral field in first order, then $3z^2 - r^2$ is excluded from the ground state and xz (B symmetry) is the only remaining possibility. The applicability of this assumption in the present case is uncertain. An energy level diagram for a d^1 ion in C_2 symmetry is shown in figure 5 for the case where the ground state has B symmetry.

The **g** and **A** tensors listed in table 1 can each be represented by four parameters: three principal values and one direction cosine specifying the orientation of the two principal axes in the plane perpendicular to the symmetry axis. On the other hand, the admixture of d orbitals in the ground state wavefunction is determined by the eigenvector corresponding to the lowest eigenvalue of the 10×10 matrix of crystal potential and spin–orbit interaction. This matrix contains five diagonal and four off-diagonal matrix elements of the C_2 crystal potential, which may be adjusted independently. Additional adjustable parameters include several orbital reduction factors and a core polarization term. It follows that ESR data alone are insufficient to determine the symmetry of the ground state.

7. Summary

From ESR measurements the spin Hamiltonian parameters of V^{4+} ions in vanadium-doped paratellurite have been determined where the impurity ion resides in a Te^{4+} site. The $3d^1$ electron exhibits an HF interaction with the $I = \frac{7}{2}$ ^{51}V nucleus and SHF interaction with two neighbouring, symmetrically arranged $I = \frac{1}{2}$ nuclei, which have been identified as protons via ENDOR. The protons add stability to the defect structure by increasing the site symmetry of the vanadium ion. This is evident from the smaller deviation of the **g** tensor's principal directions from regular rutile principal axes compared with those of other impurity ions in paratellurite, which do not exhibit neighbouring protons. This increased site symmetry probably facilitates the introduction of substitutional V^{4+} cations into the crystal.

A development of the wavefunctions for the five Kramer doublets based on group theoretical arguments for nd^1 ions in C_2 symmetry shows that three levels have wavefunctions of A symmetry, which are linear combinations of $d(x^2 - y^2)$, $d(z^2)$ and $d(yz)$, and two levels wavefunctions of B symmetry, which are linear combinations of $d(xy)$ and $d(xz)$, where x is the C_2 symmetry axis. Calculations were made in an effort to predict the measured **g** and **A** tensors assuming a ground state representing one or the other

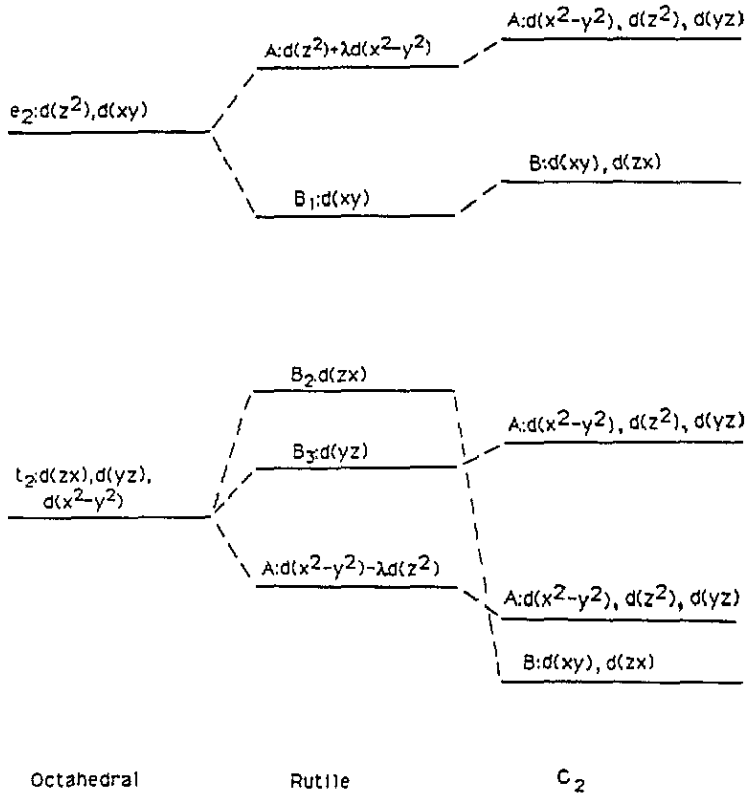

Figure 5. An energy level diagram for substitutional nd^1 cations in cubic, D_2 and C_2 symmetries, where for C_2 symmetry it has been assumed that the B representation is the ground state.

of these linear combinations, but the ground state wavefunction could not be determined from ESR data alone because of the large number of adjustable parameters. Interpretation of the measurements, however, indicates that the ground state wavefunction has its maximum density in the xz plane.

Acknowledgments

The authors are grateful to Drs I Földvári, L A Kappers and D P Madacsi for helpful discussions and to Mr P Generous for technical assistance. This research was partially supported by the US National Science Foundation under grant No INT-9222297, the National Science Research Foundation (OTKA) of Hungary under grant No T-4420, the Deutsche Forschungsgemeinschaft of Germany, the University of Connecticut Research Foundation and the University of Connecticut Computer Center.

References

[1] Watterich A, Bartram R H, Gilliam O R, Kappers L A, Edwards G J, Földvári I and Voszka R 1985 *Phys. Rev.* B **32** 2533

[2] Kröger F A, Stieltjes F and Vink H J 1959 *Philips Res. Rep.* **14** 5578
[3] Jani M G, Bossoli R B and Halliburton L E 1983 *Phys. Rev.* B **27** 2285
[4] Yip K L and Fowler W B 1975 *Phys. Rev.* B **11** 2327
[5] Hughes A E and Henderson B 1972 *Point Defects in Solids* ed J H Crawford Jr and L M Slifkin (New York: Plenum) ch 7
[6] Corradi G, Watterich A, Földvári I, Voszka R, Niklas J R, Spaeth J-M, Gilliam O R and Kappers L A 1990 *J. Phys.: Condens. Matter* **2** 4325
[7] Watterich A, Bartram R H, Gilliam O R, Kappers L A, Edwards G J, Voszka R and Cravero I 1986 *J. Phys. Chem. Solids* **47** 987
[8] Watterich A, Bartram R H, Gilliam O R, Kappers L A, Edwards G J, Földvári I and Voszka R 1986 *Phys. Lett.* **117A** 247
[9] Watterich A, Voszka R, Söthe H and Spaeth J-M 1987 *J. Phys. C: Solid State Phys.* **20** 3155
[10] Watterich A, Raksányi K, Gilliam O R, Bartram R H, Kappers L A, Söthe H and Spaeth J-M 1992 *J. Phys. Chem. Solids* **53** 189
[11] Watterich A, Bartram R H, Edwards G J, Gilliam O R, Földvári I and Voszka R 1987 *J. Phys. Chem. Solids* **48** 249
[12] Földvári I, Voszka R, Kappers L A, Hamilton D S and Bartram R H 1985 *Phys. Lett.* **109A** 303
[13] Földvári I, Cravero I, Watterich A and Morlin Z 1983 *Radiat. Eff.* **77** 161
[14] Lindquist O 1968 *Acta Chem. Scand.* **22** 977
[15] Thomas P A 1988 *J. Phys. C: Solid State Phys.* **21** 4611
[16] Schmidt F and Voszka R 1981 *Cryst. Res. Technol.* **16** K127
[17] Madacsi D P, Bartram R H and Gilliam O R 1973 *Phys. Rev.* B **7** 1817
[18] Kikuchi C, Chen J, From W H and Dorain P B 1965 *J. Chem. Phys.* **42** 181
[19] Gerritsen H J and Lewis H R 1960 *Phys. Rev.* **119** 1010
[20] Pimentel G C and McClellan A L 1960 *The Hydrogen Bond* (San Francisco, CA: Freeman)
[21] Shimizu T 1966 *Phys. Lett.* **23** 20
[22] Shimizu T 1967 *J. Phys. Soc. Japan* **23** 848